Available online at www.sciencedirect.com

ScienceDirect

MATTER AND RADIATION AT EXTREMES

Matter and Radiation at Extremes 3 (2018) 227–242

www.journals.elsevier.com/matter-and-radiation-at-extremes

Research Article

Dipole and generalized oscillator strength derived electronic properties of an endohedral hydrogen atom embedded in a Debye-Hückel plasma

C. Martínez-Flores*, R. Cabrera-Trujillo

Instituto de Ciencias Físicas, Universidad Nacional Autónoma de México, Ap. Postal 43-8, Cuernavaca, Morelos, 62251, Mexico

Received 9 January 2018; revised 12 April 2018; accepted 16 May 2018
Available online 19 July 2018

Abstract

We report electronic properties of a hydrogen atom encaged by an endohedral cavity under the influence of a weak plasma interaction. We implement a finite-difference approach to solve the Schrödinger equation for a hydrogen atom embedded in an endohedral cavity modeled by the Woods-Saxon potential with well depth V_0, inner radius R_0, thickness Δ, and smooth parameter γ. The plasma interaction is described by a Debye-Hückel screening potential that characterizes the plasma in terms of a Debye screening length λ_D. The electronic properties of the endohedral hydrogen atom are reported for selected endohedral cavity well depths, V_0, and screening lengths, λ_D, that emulate different confinement and plasma conditions. We find that for low screening lengths, the endohedral cavity potential dominates over the plasma interaction by confining the electron within the cavity. For large screening lengths, a competition between both interactions is observed. We assess and report the photo-ionization cross section, dipole polarizability, mean excitation energy, and electronic stopping cross section as function of λ_D and V_0. We find a decrease of the Generalized Oscillator Strength (GOS) when the final excitation is to an s state as the plasma screening length decreases. For a final excitation into a p state, we find an increase in the GOS as the endohedral cavity well-depth increases. For the case of the electronic stopping cross section, we find that the plasma screening and endohedral cavity effects are larger in the low-to-intermediate projectile energies for all potential well depths considered. Our results agree well to available theoretical and experimental data and are a first step towards the understanding of dipole and generalized oscillator strength dependent properties of an atom in extreme conditions encaged by an endohedral cavity immersed in a plasma medium.

PACS codes: 32.70.Cs; 62.50.-p; 37.30.+i; 52.20.-j

Keywords: Oscillator strengths; Debye-Hückel plasma; Cavities; Endohedral; Energy loss; Stopping power

1. Introduction

The study of atoms or ions under plasma environments has been a topic of great interest over the past decades due to the coupling strength of the plasma with electrons of immersed atoms and consequent modification of their electronic properties [1–3], with applications in many research areas, e.g., fusion processes [4], materials processing [5], and astrophysics environments [6]. The plasma interaction may be described by a screening potential function that incorporates the collective effects of the correlated many particles interaction processes in a plasma and has been studied exhaustively under different treatments [7,8]. e.g., by the Debye-Hückel potential [8,9], the cosine Debye-Hückel potential [10], and recently by the Coulomb potential for finite-temperature [11,12].

The photo-ionization cross section of atoms embedded in a plasma interaction has been studied previously (for a review see Janev et al. [2]). Of particular interest is the appearance of several structures consequence of the plasma environment conditions

* Corresponding author.
E-mail address: cesar@icf.unam.mx (C. Martínez-Flores).
Peer review under responsibility of Science and Technology Information Center, China Academy of Engineering Physics.

https://doi.org/10.1016/j.mre.2018.05.001

[13−15]. For example, Qi et al. [13] have studied the photo-ionization processes of the hydrogen-like ions embedded in a weak plasma, finding that the effects of the screening potential on the photo-ionization produces multiple shape and virtual-state resonances when the states are in the continuum.

Li and Ho [14] found that the resonances were sensitive to the weak plasma for critical values of the screening length, where the transition of bound states into quasi-bound states might happen.

Furthermore, Chang et al. [15] found the same photo-ionization structure resonances but for one and two electron atoms. Another property of interest is the static dipole polarizability for systems under plasma influence [16−19]. For example, Qi et al. [16] calculated the static polarizability of the hydrogen atom embedded in a Debye-Hückel plasma by means of a numerical approach finding that the static polarizability suffered a dramatic increase when the plasma screening length decreased. These results were confirmed by the work of Das [17], where he used a Runge-Kutta numerical integration method to perform the calculations.

The energy loss by heavy ions colliding with a plasma has been investigated in recent years [20−22]. Hoffmann [20] measured the energy loss in a plasma target for different heavy-ion species, finding an enhanced stopping power due to the increased energy transfer to the free plasma electrons and the charges of the projectiles inside the plasma. Zylstra et al. [21] measured the stopping power of energetic protons in an isochorically heated solid-density Be plasma, which showed an increase in energy loss relative to cold matter. Recently, an interesting application of the stopping cross section in a plasma environment was reported by Xu et al. [22], where they determined the total hydrogen density and free electron temperature of a lowly ionized hydrogen plasma by measuring the total energy loss of the beam ions.

In regards to an external confinement on an atomic system, the case of an atom encaged by a endohedral cavity is of great relevance as the consequence of its many technological applications [23]. For example, this system is of interest in material science, semiconductors, hydrogen storage, and luminescence, to mention a few [24−27]. As a consequence of the confinement, the electronic properties of atoms encaged in an endohedral cavity change, making relevant the proper modeling of the endohedral cavity under extreme conditions. One approach is to use a model potential for quantum confinement which has proved to be appropriate to describe the confinement effect. For reviews in the field, see e.g. Refs. [23,28−31]. One of the confining model potentials is the Woods-Saxon potential [32,33] which has no discontinuities at the inner and outer radii of the endohedral cavity.

Other confining potentials have been implemented in several works found in the literature, see for example Refs. [34−38].

In this work, we are interested in studying the endohedral hydrogen atom at the geometrical center of the endohedral cavity, as a first order approximation. We combine the Debye-Hückel model potential for a weak plasma with the addition of an endohedral confinement in order to study the energy levels and wave functions, with a consequent change in the Dipole Oscillator Strength (DOS) and Generalized Oscillator Strength (GOS) and related hydrogenic electronic properties. The properties under study are the photo-ionization cross section, static dipole polarizability, the mean excitation energy, and the stopping cross section (projectile energy loss). To our knowledge, there is no literature reporting the GOS properties for an endohedral hydrogen atom embedded in a weak plasma interaction. An example of a system under these characteristics could be an endohedral hydrogen atom encaged by a buckyball ($H@C_{60}$) immersing in a weak hydrogen interstellar plasma. It has been confirmed recently the existence of buckyballs in space [39] which has resolved some issues concerning spectral lines observed in near-by stars. Another example could be hydrogen storage by fullerene immersing in a plasma e.g. hydrogen confinement in a C_n molecule by a spherical theta pinch devise [22,40].

Our work is presented as follows. In Sec. 2, we provide the theoretical approach used to study the influence of the plasma environment on an endohedral hydrogen atom. In Sec. 3, our results and findings are discussed. In Sec. 4, we give our conclusions and perspectives. We use atomic units unless physical units are explicitly stated.

2. Theory

2.1. Confinement model

The non-relativistic time-independent Schrödinger equation is used to describe the hydrogen atom encaged by an endohedral cavity embedded in a weak plasma interaction. The hydrogen atom is at the geometrical center of the cavity and the one active electron is described by a Debye-Hückel screening interaction. The spherical symmetry of the problem permit us to write the wave-function as $\psi(r,\ \theta,\ \phi) = R_{nl}(r)Y_l^m(\theta,\phi) = [u_{nl}(r)/r]Y_l^m(\theta,\phi)$, where $R_{nl}(r)$ is the radial wave-function and $Y_l^m(\theta,\phi)$ are the spherical harmonics. The Schödinger equation for the cavity and plasma confinement is reduced to a one-dimension equation in terms of the radial variable

$$\left[-\frac{1}{2}\frac{\mathrm{d}^2}{\mathrm{d}r^2}+\frac{l(l+1)}{2r^2}+V_{\mathrm{D}}(r)+V_c(r)\right]u_{nl}(r)=E_n u_{nl}, \tag{1}$$

where $V_{\mathrm{D}}(r)$ is the Debye plasma screening potential [7,8],

$$V_{\mathrm{D}}(r)=-\frac{Z}{r}\exp(-r/\lambda_{\mathrm{D}}), \tag{2}$$

with Debye screening length given by $\lambda_{\mathrm{D}} = [4\pi(1+Z^*)ne^2/k_{\mathrm{B}}T]^{-1/2}$, k_{B} is the Boltzmann constant, n the density of plasma electrons, T the temperature, Z^* the effective charge of the ions in the embedded plasma, and Z the hydrogenic nuclei charge. The Debye-Hückel model is valid for weak plasmas, i.e. where $\Gamma = (Ze)^2(4\pi n/3)^{1/3}/k_{\mathrm{B}}T < 1$ is fulfilled [3,8].

The confining potential, $V_{\mathrm{c}}(r)$, used to describe the endohedral cavity is given by the Woods-Saxon potential [32],

$$V_c(r) = \frac{V_0}{1+\exp\{-[r-(R_0+\Delta)]/\gamma\}} - \frac{V_0}{1+\exp[-(r-R_0)/\gamma]} \quad (3)$$

In this model, the endohedral cavity has an inner radius R_0, a spherical shell thickness Δ, a potential well depth V_0, and a smoothing parameter γ. We should notice here that our model potential is an static one where any effects of the plasma on the endohedral cavity are neglected, since we are only interested in studying the effects of the plasma and the confinement on the endohedral hydrogenic atom. This first approximation can be improved by using a dynamic potential, which is out of the scope in the present study.

2.1.1. Finite differences approach

As the numerical approach to solve Eq. (1) has been previously reported [41], here we summarize our procedure to find the eigenvalues and eigenfunctions. We use the finite-difference approach, which consists in discretizing the function $u(r)\to u_k$ and $r\to r_k$, known at the k-th point on a numerical grid, with $k=0$ corresponding to u_0 and $k=N+1$ to u_{N+1}, which are the boundary conditions of the system [42]. We implement the finite-difference approach centered at the midpoint such that Eq. (1) is rewritten as

$$\boldsymbol{H}\phi = E\phi \quad (4)$$

Here $\boldsymbol{H}$ is a tridiagonal symmetric matrix with N eigenvalues and eigenfunctions and ϕ is related to $\boldsymbol{u}$ by means of a linear transformation [41].

2.2. Physical properties

Once the set of eigenvalues and eigenfunctions are determined, the electronic properties can be calculated.

Dipole and generalized oscillator strengths. The GOS accounts for the probability transition from the ground state to a particular excited state for a given momentum transfer, $\boldsymbol{q}$, and is defined as

$$F_{n0}(\boldsymbol{q}) = \frac{2}{q^2}(E_n-E_0)\left|\langle\psi_n(\boldsymbol{r})\left|e^{i\boldsymbol{q}\cdot\boldsymbol{r}}\right|\psi_0(\mathbf{r})\rangle\right|^2 \quad (5)$$

Here ψ_0 and ψ_n are the initial and final states, with eigenvalues E_0 and E_n, respectively.

To verify that our numerical approach has rendered a complete set of states, the Bethe's sum rule (BSR) [43,44], $\sum_n F_{n0}(\boldsymbol{q}) = N_e$, must be fulfilled and is valid for any value of $\boldsymbol{q}$. Here N_e is the number of electrons.

By taking into account the spherical symmetry of the system and considering a s-initial state, the GOS is reduced to [41],

$$F_{n0} = \frac{2}{q^2}(E_n-E_0)|M_{n0}(q)|^2 \quad (6)$$

where

$$M_{n0}(q) = i^l\sqrt{2l+1}\int_0^\infty j_l(qr)u^*_{nl}(r)u_{10}(r)dr \quad (7)$$

is the atomic form factor and $j_l(x)$ is the spherical Bessel function of order l, with l the angular momentum quantum number of the final n-state.

In the special case when $q\to 0$, the GOS reduces to the DOS, i.e.

$$f_{n0} = 2(E_n-E_0)|\langle\psi_n(\boldsymbol{r})|\boldsymbol{r}\cdot\hat{\varepsilon}|\psi_0(\boldsymbol{r})\rangle|^2 \quad (8)$$

where $\hat{\varepsilon}$ is the direction of the momentum transfer or the polarization of the electromagnetic radiation. Under spherical symmetry of the system, Eq. (8) is reduced to [44,45],

$$\bar{f}_{n0} = \frac{2}{3}(E_n-E_0)|\langle R_n(r)|r|R_0(r)\rangle|^2 \quad (9)$$

In this particular case, the BSR is known as the Thomas-Reiche-Kuhn (TRK) sum rule [43], $\sum_{n_f}\bar{f}_{n_f,n_i} = N_e$.

Photo-ionization cross section. Once the DOS has been obtained, we proceed to calculate the DOS dependent properties. We start with the study of the photo-ionization cross section (PCS), which is defined as

$$\sigma_{nl}(h\nu) = \pi^2\left(\frac{e^2\hbar}{2mc}\right)\frac{d\bar{f}_{n0}}{dE} \quad (10)$$

where $d\bar{f}_{n0}/dE$ is the dipole oscillator strength density within the energy E and $E+dE$. This requires that the pseudo-continuum wave-function of the final state must be normalized with respect to the energy, $u\to u_E$, i.e.

$$\int u^*_{E'}(r)u_E(r)dr = \delta(E'-E) \quad (11)$$

such that

$$\frac{d\bar{f}_{n0}}{dE} = \frac{2}{3}(E_n-E_0)|\langle R_{E_n}(r)|r|R_0(r)\rangle|^2 \quad (12)$$

with $R_E(r) = u_E(r)/r$. In our particular case, we follow the procedure of Ugray et al. [46] to normalize the radial wave-function of the pseudo-continuum spectrum as follows

$$R_{E_n}(r) = \sqrt{\frac{2}{E_{n+1}-E_{n-1}}}R_n(r) \quad (13)$$

where $E_{n+1}(E_{n+1})$ is the energy of the adjacent above (below) pseudo-continuum excited state to E_n and $R_n(r)$ is our numerical-box normalized wave-function. With this energy normalization, we evaluate Eq. (10) to find the photo-ionization cross section under several confinement conditions through Eq. (12).

Static dipole polarizability. The static dipole polarizability is defined through the DOS (Eq. (9)), and is given as

$$\alpha_s = \sum_n \frac{\overline{f}_{n0}}{(E_n - E_0)^2} \tag{14}$$

Mean excitation energy. A parameter that characterizes the amount of energy loss when a swift heavy projectile penetrates a target is given by the mean excitation energy, I_0, as defined by Bethe [47].,

$$\ln I_0 = \frac{\sum_n \overline{f}_{n0} \ln(E_n - E_0)}{\sum_n \overline{f}_{n0}} \tag{15}$$

Electronic stopping cross section. The electronic stopping cross section, S_e, for a projectile of mass M_p, atomic number Z_p, and velocity v, colliding with a target with N_e bound electrons of mass m_e, is given as

$$S_e(v) = \frac{4\pi e^4 Z_p^2}{m_e v^2} L(v) \tag{16}$$

where $L(v)$ is the stopping number. In Bethe's theory [47], the stopping number is given in terms of the GOS as

$$L(v) = \sum_{n=1} \int_{q_{\min}(n)}^{q_{\max}(n)} F_{n0}(q) \frac{dq}{q} \tag{17}$$

The integration over q is carried out between a minimum and maximum momentum transfer during the collision with [44],

$$q_{\min}^{\max}(n) = \frac{M_p v}{\hbar} \left[1 \pm \sqrt{1 - \frac{2(E_n - E_0)}{M_p v^2}} \right] \tag{18}$$

Here E_0 and E_n are the initial and final energy levels of the system, respectively.

2.3. Numerical implementation

We solve Eq. (4) in a grid box that extends from $r = 0$ to $r = 500$ a.u. with a total number of $N = 2000$ points spaced logarithmically in this range. This logarithmic grid allows us to have a better description of the wave-function cusp at the origin, and a good number of continuum states. We have calculated the GOS for values of the momentum transfer q up to 30 a.u. in steps of $\Delta q = 0.1$ a.u. and we have found that a value of l up to $l_{\max} = 100$ fulfills the TRK sum rule up to 5 decimals. This means that we have a total of 200 000 excited states to describe the GOS electronic properties of the endohedral cavity in a plasma for each well depth V_0 and λ_D. The accuracy of our finite-difference approach is a function of the number of points in the grid and their spacing, e.g., for the free hydrogen atom, we obtain eigenvalues with precision up to the 5-th decimal place. With an increase of points in the grid the precision increases but so does the computational cost.

For the case of the endohedral cavity, we use $R_0 = 5.8$ a.u., $\Delta = 1.89$ a.u., and $V_0 = 0.302$ a.u., as proposed by Xu et al. [48,49] for an endohedral cavity. We assume that the cavity will remain unaltered by the plasma conditions, i.e its electronic structure and geometry are independent of the value of λ_D. In order to avoid the discontinuity at $r = R_0$ and $r = R_0 + \Delta$, we use a smoothing parameter $\gamma = 0.1$, as suggested by Dolmatov et al. [33]. We complement our study by reporting the electronic properties of interest for other selected well depth values of $V_0 = 0$, 0.7, and 1.0 a.u., that represent different electronic configurations of an endohedral cavity. The choice of the value of $V_0 = 0$ corresponds to no cavity, $V_0 = 0.7$ to the cavity depth for the first avoiding crossing between 2s and 1s state [29], and $V_0 = 1.0$ to when the 2s hydrogen state is emulating the 1s state [29]. For each potential well depth, we present our results as a function of selected screening length λ_D ranging from 0.1 to 100,000 a.u. This last value is our numerical limit to no plasma.

Our approach has been implemented in a FORTRAN 95 code that calculates the eigenvalues, eigenfunctions, and physical properties of the system.

3. Results

In order to relate the order of magnitude of the plasma density, as a function of the Debye screening length λ_D, in Fig. 1, we show the electron plasma density for several temperatures as a function of λ_D in a.u. Examples of weakly coupled plasmas (thick blue-lines) are those occurring in fusion plasma ($T \sim 6 \times 10^6 - 10^7$ K, $n \sim 10^{22} - 10^{26}$ cm^{-3}), laser-produced plasma ($T \sim 5 \times 10^5 - 3 \times 10^6$ K, $n \sim 10^{19} - 10^{21}$ cm^{-3}), and stellar atmosphere ($T \sim 6 \times 10^3 - 6 \times 10^4$ K, $n \sim 10^{15} - 10^{18}$ cm^{-3}) [3,15,16]. As shown in Fig. 1, the yellow shaded region is where the weak plasma condition of our model is fulfilled.

3.1. Energy levels

In Fig. 2(a)–(d), we show the energy levels of the hydrogen atom encaged by an endohedral cavity in a Debye-Hückel plasma. The energies of 1s–4s and 2p to 4p are shown as a function of screening length λ_D for several potential well

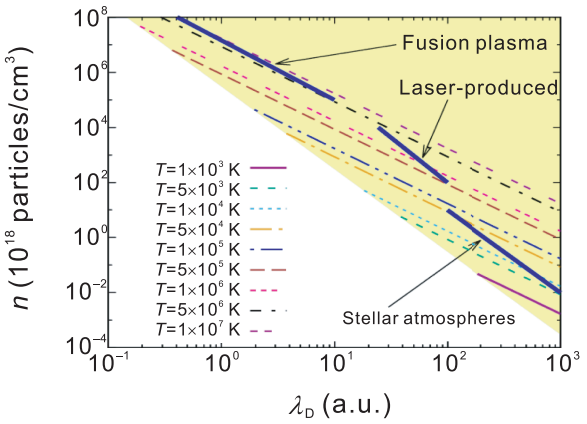

Fig. 1. The density of plasma electrons, n (cm^{-3}), as a function of the screening length, λ_D (a.u.), for several plasma temperatures T (K). The thick lines are example regions for fusion plasma, laser-produced plasma, and stellar atmospheres where our model is applicable (yellow shaded area). See text for discussion.

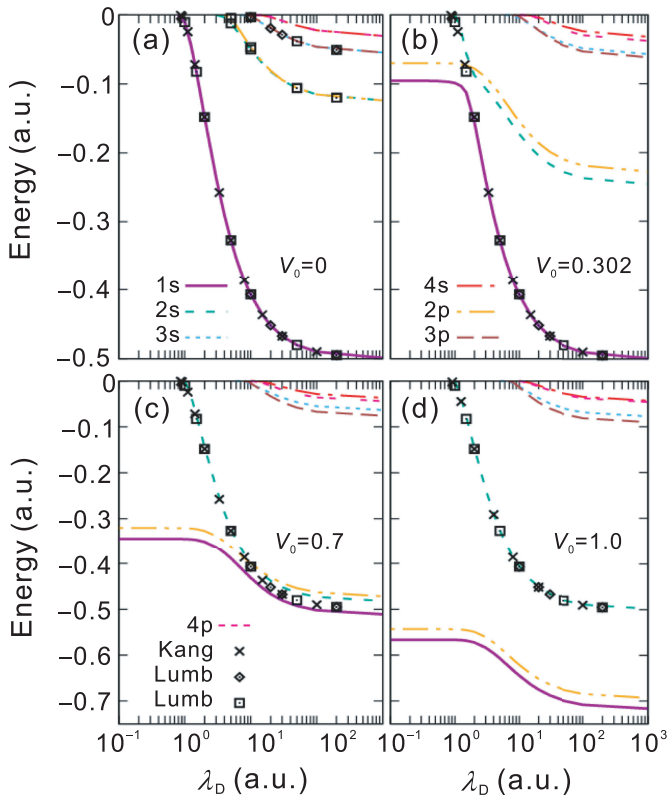

Fig. 2. Hydrogen atom energy levels as a function of the screening length λ_D for the 1s–4s and 2p to 4p states when encaged by an endohedral cavity embedded in a Debye-Hückel plasma for selected well depths V_0. The well depths considered are: (a) $V_0 = 0.0$, (b) $V_0 = 0.302$, (c) $V_0 = 0.7$, and (d) $V_0 = 1.0$ a.u. The results are compared to those of Kang et al. (×) [50], Lumb et al. (⋄) [51], and Lumb et al. (□) [52] without endohedral cavity ($V_0 = 0$). See text for discussion.

depths V_0. The results for $V_0 = 0$ a.u. (the endohedral cavity is not present and the interaction is only through a Debye-Hückel plasma) are shown in Fig. 2(a). For the case $\lambda_D = \infty$ a.u., we obtain the well-known energy values of the hydrogen atom. For $\lambda_D < 0.84428$ a.u., the 1*s* state is not bound anymore, i.e. it is delocalized in the continuum. For the other states, there is a delocalization of the excited states for different screening lengths, as observed in Fig. 2(a) in agreement with previous findings [16,50–53]. In Fig. 2, we show the results of Kang et al. [50] (× symbols for the case of $V_0 = 0$), Lumb et al. [51] (⋄), and Lumb et al. [52] (□), observing an excellent agreement when compared to our 1s state results (solid line).

By adding the endohedral cavity, a new and novel system is obtained. In Fig. 2(b), we show the results for a well depth with $V_0 = 0.302$ a.u. Here, we observe that the 1s and 2p states remain bound to the cage for $0.1 < \lambda_D < 1$ a.u. with almost a constant energy, thus breaking the delocalization of the 1s state. Here both states are confined into the endohedral cage due to the weak effects of the plasma environment when compared to the endohedral cavity (see below). In the same figure, we observe that the 2s state is bound for values of the screening length $\lambda_D > 1.09899$ a.u. in contrast with the results shown in Fig. 2(a) for the same state which is bound for $\lambda_D > 3.26010$ a.u. As we notice, higher excited states are affected by the presence of the endohedral cavity and remain bound for different values of the screening length, as observed in Fig. 2(b). For values of $\lambda_D > 1000$ a.u. the plasma screening effect on the energy levels is negligible and only the endohedral cavity potential produces an effect. In Fig. 2(c), we observe a significant change in the 1s, 2s, and 2p energy levels when the depth of the endohedral cavity is increased to $V_0 = 0.7$ a.u. The 1s state is bound by the endohedral cage for all screening length values λ_D and the 2s state is bound within the hydrogen atom and takes the characteristics of the unconfined 1s energy state without endohedral cavity for large screening length values, in agreement to Connerade findings [29]. However, the 2s state starts to be delocalized as the screening length is decreased. Also, we find that the 2s energy level behaves as the 1s energy when there is no cavity for $\lambda_D < 7$ a.u (see Fig. 2(a)). and our results match those of Kang et al. [50], Lumb et al. [51], and Lumb et al. [52]. In the same figure, we observe a similar behavior for the 1s and 2p energy states becoming constant for a screening length lower than $\lambda_D < 5.0$ a.u. similar to the case of $V_0 = 0.302$ a.u. Both states are confined in the endohedral cavity due to the weakening effect of the plasma interaction in comparison to the endohedral cavity.

In Fig. 2(d), we show the results for a well depth of $V_0 = 1.0$ a.u. For values of the screening length $\lambda_D < 1$ a.u., the 1s and 2p states have a constant energy and are bound to the endohedral cavity. The 2s state is localized at the H nucleus mimicking a 1s hydrogen state. Again, we observe in Fig. 2(d) an excellent agreement between Kang et al. [50], Lumb et al. [51], and Lumb et al. [52] results for no cavity and our 2*s* energy states. With the increase of the well depth, the 1s and 2p energy states are modified significantly for large values of λ_D reaching $E_{1s} = -0.71761$ a.u. and $E_{2p} = -0.69407$ a.u., respectively. We observe from Fig. 2(b)–(d) that the behavior of the 1s and 2p energy levels produce an energy difference $(E_{2p} - E_{1s})$ which becomes constant as the well depth is increased and the screening length is decreased. The previous characteristic will be of relevance in the understanding of the dipole properties described in the next sections.

In Table 1, we provide the critical values of the screening length for the threshold transition from bound to continuum states. We also provide Qi et al. [13] values for $V_0 = 0$ in parenthesis next to our values for reference, showing good

Table 1
Critical values for the screening length, λ_D, at the delocalization of the energy levels for several confinement well depths. The results within parenthesis correspond to the case of only plasma interaction from the work of Qi et al. [13].

E_{nl}	$V_0 = 0.0$	$V_0 = 0.302$	$V_0 = 0.7$	$V_0 = 1.0$
1s	0.84428 (0.83990)	–	–	–
2s	3.26010 (3.22255)	1.09899	1.05333	1.02574
3s	7.29763 (7.17173)	6.51887	6.16438	5.74346
4s	12.99288 (12.68644)	12.57321	11.88938	10.59805
2p	4.54257 (4.54095)	–	–	–
3p	8.84610 (8.87222)	8.65046	8.22359	7.43027
4p	14.78249 (14.73072)	13.86346	11.92049	10.64895

consistent agreement. We attribute the slight numerical difference between both approaches to the different approaches used in both methods.

In Table 2, we provide the values of the 1s and 2p energy states and the corresponding DOS for several well depths and selected values of the screening length, λ_D, for reference purposes. We compare our results with those given by Lin and Ho [14] for no endohedral cavity showing an excellent agreement.

3.2. Wave-functions

The previous electronic energy-level results can be understood better by analyzing the behavior of the wave-function. In Fig. 3, we show the 1s wave-function for the H atom in an endohedral cavity embedded in a Debye-Hückel plasma for several well depths, V_0, and screening length λ_D, as a function of the radial electron position. In Fig. 3(a) the analytic wave-function is represented by ($\circ$) symbols for $V_0 = 0$ a.u. and $\lambda_D = \infty$, i.e. the free hydrogen atom, observing an excellent agreement with our numerical results. As λ_D decreases, we observe that the wave-function width is increased and the amplitude is decreased, such that the wave-function becomes delocalized for $\lambda_D < 0.84428$ a.u. In Fig. 3(b), we show the case for $V_0 = 0.302$ a.u. Here we observe that the wave-function starts to change for screening lengths $\lambda_D < 3$ a.u. and it presents a bump around $6 < r < 8$ a.u., the region of the endohedral cavity. Thus, the electron becomes localized within the endohedral cavity as observed in Figs. 2(b) and 3(b). For the case of a well depth of $V_0 = 0.7$ a.u., near the first avoided crossing for the endohedral system without plasma interaction [29], we observe, in Fig. 3(c), that the wave-function is shared between the hydrogen atom and the endohedral cavity and the electron becomes completely bound in the endohedral cavity

Table 2
Energy values for the 1s and 2p states, as well as the corresponding DOS (f_{2p}) for a hydrogen atom in an endohedral cavity embedded in a Debye-Hückel plasma for several selected values of the well depths, V_0, and the plasma screening length, λ_D, as obtained with our FD approach. The results in parenthesis correspond to those given by Lin and Ho [14].

λ_D	$V_0 = 0.0$			$V_0 = 0.302$		
	E_{1s}	E_{2p}	f_{2p}	E_{1s}	E_{2p}	f_{2p}
0.1	–	–	–	−0.09528	−0.06988	0.80914
0.3	–	–	–	−0.09540	−0.06989	0.81148
0.5	–	–	–	−0.09572	−0.06991	0.81717
0.8	–	–	–	−0.09696	−0.07014	0.83451
1.0	−0.01029	–	–	−0.09874	−0.07056	0.85312
2.0	−0.14812	–	–	−0.15468	−0.07754	0.40545
	(−0.148117)	–	–	–	–	–
3.0	−0.23683	–	–	−0.23840	−0.08992	0.18145
	(−0.236833)	–	–	–	–	–
4.0	−0.29092	–	–	−0.29181	−0.10308	0.15037
	(−0.290920)	–	–	–	–	–
5.0	−0.32681	−0.00410	0.19334	−0.32748	−0.11510	0.14303
	(−0.326809)	(−0.004102)	–	–	–	–
8.0	−0.38588	−0.03277	0.33444	−0.38635	−0.14217	0.14226
	(−0.385879)	(−0.032768)	–	–	–	–
10	−0.40706	−0.04653	0.36301	−0.40749	−0.15447	0.14380
15	−0.43653	−0.06830	0.39147	−0.43692	−0.17423	0.14646
20	−0.45182	−0.08074	0.40182	−0.45219	−0.18578	0.14779
50	−0.48030	−0.10596	0.41370	−0.48066	−0.20987	0.14962
100	−0.49008	−0.11525	0.41555	−0.49043	−0.21897	0.14994
∞	−0.49999	−0.12499	0.41619	−0.50035	−0.22865	0.15005
		$V_0 = 0.7$			$V_0 = 1.0$	
0.1	−0.34414	−0.32063	0.71632	−0.56632	−0.54331	0.69922
0.3	−0.34414	−0.32064	0.71644	−0.56632	−0.54331	0.69924
0.5	−0.34416	−0.32064	0.71671	−0.56632	−0.54331	0.69927
0.8	−0.34429	−0.32073	0.71754	−0.56639	−0.54338	0.69938
1.0	−0.34459	−0.32099	0.71838	−0.56662	−0.54359	0.69950
2.0	−0.35096	−0.32693	0.72557	−0.57232	−0.54921	0.70044
3.0	−0.36303	−0.33835	0.73564	−0.58357	−0.56037	0.70140
4.0	−0.37618	−0.35069	0.74578	−0.59581	−0.57253	0.70216
5.0	−0.38845	−0.36204	0.75295	−0.60710	−0.58376	0.70273
8.0	−0.41736	−0.38786	0.73967	−0.63281	−0.60939	0.70370
10	−0.43112	−0.39972	0.70901	−0.64465	−0.62119	0.70403
15	−0.45355	−0.41892	0.63689	−0.66382	−0.64031	0.70443
20	−0.46655	−0.43023	0.59624	−0.67511	−0.65159	0.70460
50	−0.49268	−0.45403	0.54145	−0.69890	−0.67536	0.70480
100	−0.50213	−0.46308	0.53249	−0.70795	−0.68441	0.70483
∞	−0.51193	−0.47274	0.52937	−0.71761	−0.69407	0.70485

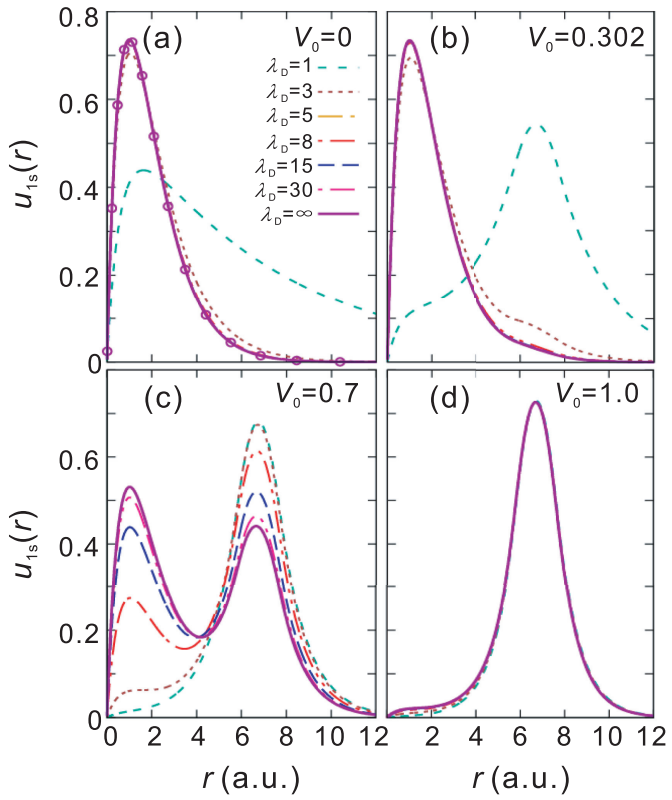

Fig. 3. Radial wave function for the 1s state of the Hydrogen atom in an endohedral cavity embedded in a Debye-Hückel plasma for selected potential well depths: (a) $V_0 = 0.0$, (b) $V_0 = 0.302$, (c) $V_0 = 0.7$, and (d) $V_0 = 1.0$ a.u., for several screening lengths λ_D. The ($\circ$) symbols are the analytic results for the free hydrogen atom. See text for discussion.

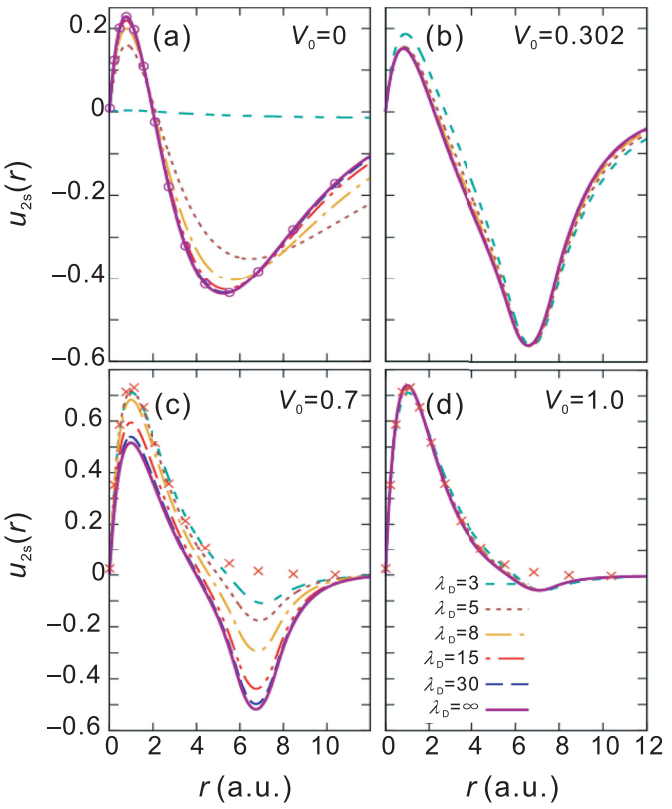

Fig. 4. Radial wave function for the 2s state of the Hydrogen atom in an endohedral cavity embedded in a Debye-Hückel plasma for selected potential well depths: (a) $V_0 = 0.0$, (b) $V_0 = 0.302$, (c) $V_0 = 0.7$, and (d) $V_0 = 1.0$ a.u., for several screening lengths λ_D. In (a), the ($\circ$) symbols represent the free hydrogen atom 2s wave-function. In (c) and (d), the ($\times$) symbols are the free hydrogen 1s wave-function.

region for $6 < r < 8$ a.u. and $\lambda_D < 1$ a.u. Finally, in Fig. 3(d), we show the results for $V_0 = 1.0$ a.u., finding that the Debye-Hückel plasma influence is almost negligible on the 1s wave-function for all values of λ_D, consequence of the strong effect of the endohedral cavity.

In Fig. 4, we show the wave-function for the 2s state of the endohedral H atom in a Debye-Hückel plasma. For a well depth of $V_0 = 0$ a.u. and $\lambda_D \to \infty$ a.u., we obtain an excellent agreement with the analytic free hydrogen wave-function, as shown in Fig. 4(a) by ($\circ$) symbols. As the screening length is decreased, the wave-function becomes more diffuse and diminishes its amplitude until the electron becomes delocalized. In Fig. 4(b), we show the case of a cavity with $V_0 = 0.302$ a.u., noticing a significant change in the 2s wave-function in comparison with the free case shown in Fig. 4(a). Here, the 2s wave-function shows a strong confinement within the endohedral cavity for $6 < r < 8$ a.u. with a minimal effect from the plasma interaction. In the case of a well depth with $V_0 = 0.7$ a.u., near the avoiding crossing for a pure endohedral confinement, we observe an interesting and unreported behavior for the confined electron wave-function as shown in Fig. 4(c). For small λ_D, the 2s state is bound to the H nuclei and resembles the 1s free hydrogen wave-function, as seen by the good agreement for the free case shown by ($\times$) symbols. As λ_D increases, the wave-function splits partially between the endohedral cage and the hydrogen atom nuclear position due to the strong influence of the endohedral potential well as observed in Fig. 4(c). For a well depth of $V_0 = 1.0$ a.u., in Fig. 4(d), we observe that the influence of the Debye-Hückel plasma on the 2s state is minimal. The wave-function is bound to the H atom due to the strong effect of the endohedral cavity for all values of the plasma screening, and the 2s wave-function exhibits the characteristics of the 1s state of an unconfined hydrogen atom, as observed in Fig. 3(d) shown by ($\times$) symbols.

In Fig. 5, we show the 2p wave-function of the H atom within an endohedral cavity in a Debye-Hückel plasma. For a well depth of $V_0 = 0$ a.u. and $\lambda_D \to \infty$ a.u. (free hydrogen atom), in Fig. 5(a), we observe an excellent agreement between our numerical and the analytic results shown by ($\circ$) symbols. Similar to the previous case, we find that as λ_D decreases, the 2p wave-function becomes more delocalized. When the endohedral cavity is present with $V_0 = 0.302$ a.u., Fig. 5(b) shows that the wave-function is confined within the endohedral cage and the screening potential has a minimal effect in the 2p state. In Fig. 5(c) and (d), we show the wave-function for well depths $V_0 = 0.7$ and $V_0 = 1.0$ a.u.,

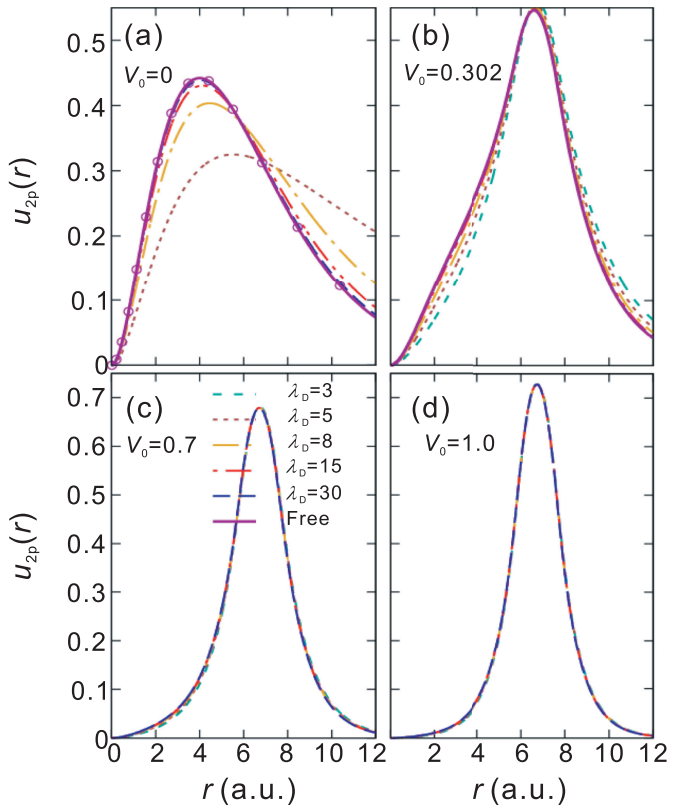

Fig. 5. Radial wave function for the 2p state of the Hydrogen atom in an endohedral cavity embedded in a Debye-Hückel plasma for selected potential well depths: (a) $V_0 = 0.0$, (b) $V_0 = 0.302$, (c) $V_0 = 0.7$, and (d) $V_0 = 1.0$ a.u., for several screening lengths λ_D. Here, the ($\circ$) symbols are the 2p free hydrogen wave-function.

respectively, finding that the effect of the Debye-Hückel plasma interaction on the 2p wave-function is negligible and its behavior is completely dominated by the endohedral cavity.

Thus, we partially conclude that the electron will be localized in different regions of the cavity depending on the strength of the Debye-Hückel potential or the endohedral cavity well depth. In consequence, the electronic properties will be different due to the competition between both interactions.

3.2.1. Dipole oscillator strength

In Fig. 6, we show the DOS for the 1s→2p transition, f_{2p}, for several well depths V_0, as a function of the screening length λ_D. In the same figure, we compare our numerical results (solid line) with the Debye-Hückel results (no endohedral cavity, $V_0 = 0$) of Saha et al. [53] ($\triangle$), Qi et al. [16] ($\square$), Kang et al. [50] ($\times$), and Lumb et al. [51] ($\diamond$), finding an excellent agreement. In the absence of the endohedral cavity, and for $\lambda_D \to \infty$ a.u., we recover the well-known free hydrogen value of $f_{2p} = 0.41619$. As the screening length decreases until $\lambda_D = 4.54257$ a.u., where there is not anymore a bound f_{2p} transition, the value of f_{2p} decreases, i.e. the 2p state becomes delocalized. When the endohedral cavity is present with a well depth of $V_0 = 0.302$ a.u., we observe a significant change in the 1s→ 2p transition for large screening lengths

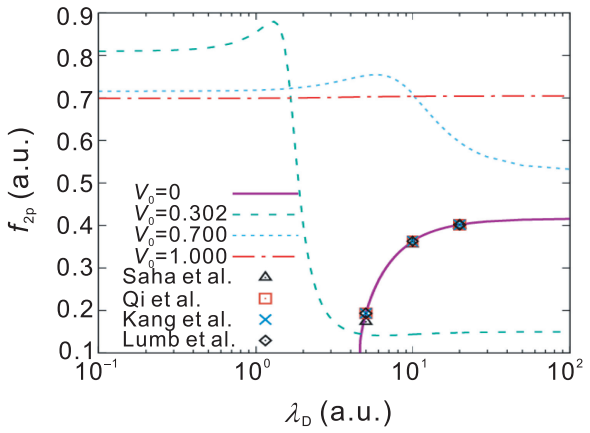

Fig. 6. Dipole oscillator strength for the 1s → 2p transition, f_{2p}, of the H atom encaged by an endohedral cavity in a Debye-Hückel plasma for selected well depths V_0, as a function the screening length λ_D. The ($\triangle$) symbols are those from Saha et al. [53], the ($\square$) symbols are from Qi et al. [16], the ($\times$) symbols are from Kang et al. [50], and the ($\diamond$) symbols are from Lumb et al. [51] for the case $V_0 = 0$. See text for discussion.

where the f_{2p} takes a value of 0.15 and increases for the region $1 < \lambda_D < 3$ a.u., reaching a value of $f_{2p} \simeq 0.81$ for $\lambda_D < 1$ a.u. This constant value is due to the behavior exhibited by the 1s and 2p energy levels (Fig. 2) and wave-functions (Figs. 3 and 5). For a well depth of $V_0 = 0.7$ a.u., we observe a similar but less prominent behavior as the previous case. For $\lambda_D < 1.5$ a.u., we obtain an average value of $f_{2p} = 0.71$, which is consequence of the confinement of 1s and 2p states in the endohedral cavity by the potential well and strong plasma interaction. As we observe from Fig. 6, the largest change in the f_{2p} is given for screening lengths between $5 < \lambda_D < 30$ a.u. where the influence of the plasma decreases and the endohedral potential becomes dominant. Here the abrupt change is a consequence of the 1s wave-function being partially confined by the endohedral cavity shell and the H atom as well as the 2p wave-function being completely confined in the endohedral region (see Figs. 2(c), 3(c) and 5(c)). When the well depth of the endohedral cavity is $V_0 = 1$ a.u., the f_{2p} is almost constant for all the screening lengths between $0.1 < \lambda_D < \infty$ a.u. as shown in Fig. 6 with a value of around 0.7. Here, the wave-functions for the 1s and 2p states are completely confined in the endohedral cavity, as observed in Figs. 3(d) and 5(d). Thus, the endohedral cavity influence on the f_{2p} is dominant while the plasma screening effect is negligible. So, we conclude that the effect of the plasma is to weaken the 1s→ 2p transition as λ_D decreases while adding the endohedral cavity strengthens the transition emission as λ_D decreases, which becomes the dominant emission line.

3.3. DOS-dependent properties

3.3.1. Photo-ionization cross section

The large changes of the energy-levels, wave-functions, and DOS are reflected on the dipole oscillator dependent properties. In Fig. 7(a)–(d), we show the photo-ionization cross section (PCS) for the H atom within an endohedral cavity

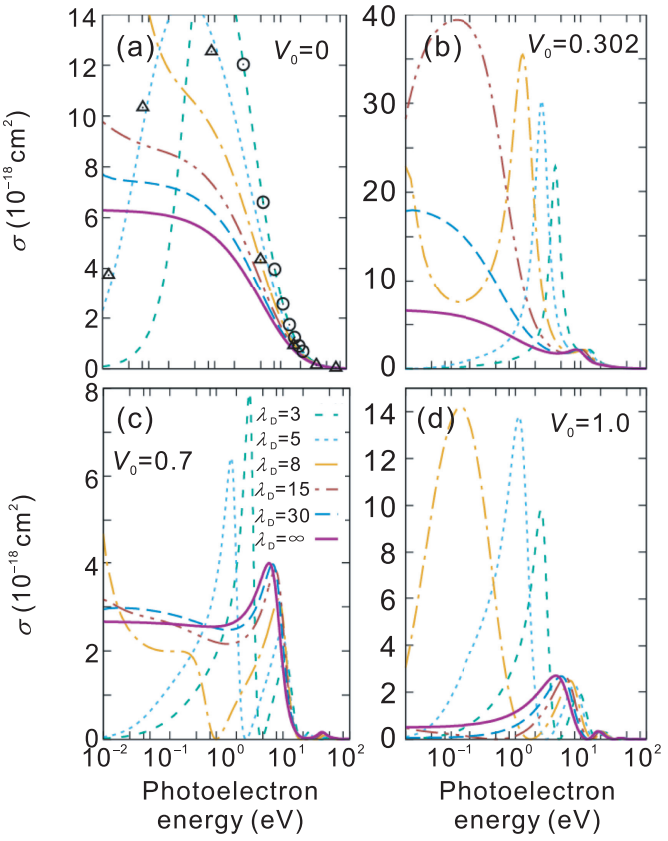

Fig. 7. Photo-ionization cross section for a H atom within an endohedral cavity embedded in a Debye-Hückel plasma environment for selected well depths V_0 and for several screening lengths, λ_D, as a function of the photo-electron energy. The (∘) symbols are the theoretical results of Lin and Ho [14] for $\lambda_D = 3$ a.u. and the (△) symbols are the theoretical results of Qi et al. [13] for $\lambda_D = 5$ a.u. See text for discussion.

embedded in a Debye-Hückel plasma for selected well depths V_0 and screening lengths λ_D as a function of the photo-electron energy. Here, we show the results for $V_0 = 0$, 0.302, 0.7, and 1 a.u., as well as for $\lambda_D = 3$, 5, 8, 15, 30, and ∞ a.u.. In Fig. 7(a), we show the case of $V_0 = 0$ a.u. (no endohedral cavity) in solid line, finding an increase of the PCS as the screening length is decreased for low-to-intermediate photo-electron energies. In the same figure, we observe the appearance of resonant structures as λ_D approaches the critical screening length of $\lambda_D = 4.54257$ a.u. for the 2p state to become unbound [16] (see Table 1). For $\lambda_D \to \infty$ a.u., we obtain the free case result in agreement with the well-known analytic results of Bethe [43]. The (∘) symbols are the results given by Lin and Ho [14] for $\lambda_D = 3$ a.u. and the (△) symbols are the theoretical results of Qi et al. [13] for a pure hydrogen plasma ($V_0 = 0$, no cavity) and $\lambda_D = 5$ a.u. finding an excellent agreement with our results. In Fig. 7(b)–(d), we observe the appearance of multiple structures in the PCS when the endohedral cavity is present for a given screening length. These structures, known as Cooper resonances, occur due to constructive interference of the photo-electron waves scattered-off by the endohedral cage and the outgoing photo-electron wave [54–56]. We find that Cooper resonances are strongly dependent on the screening length and on the endohedral cavity well depth, as observed in Fig. 7(b)–(d). In Fig. 7(b), for $V_0 = 0.302$ a.u., we observe the increase of the PCS for large values of λ_D for a given photo-electron energy and the Cooper resonances position moves towards high photo-ionization energies as λ_D is decreased. For the case of $V_0 = 0.7$ a.u., in Fig. 7(c), the Cooper resonances decrease and are shifted to larger values of photo-electron energies. In Fig. 7(d), we show the results for $V_0 = 1.0$ a.u.. Here the PCS curve increases for low values of the screening length.

3.3.2. Static dipole polarizability

In Fig. 8, we show the static dipole polarizability, α_s, as a function of the screening length λ_D for selected well depths V_0. For the free case, i.e. $V_0 = 0$ a.u. and $\lambda_D \to \infty$, we find that $\alpha_s = 4.49995$ a.u., in excellent agreement with the free hydrogen result [45]. Here, we also compare to the findings of Qi et al. [16] (△) showing an excellent agreement with our results. The contributions to α_s from the bound and continuum spectra are $\alpha_s = 3.66172$ a.u. and $\alpha_s = 0.83823$ a.u., respectively, also in excellent agreement to the results reported by Qi et al. [16]. When the screening length decreases to $\lambda_D = 5$ a.u., the static polarizability increases to a value of $\alpha_s = 5.27631$ a.u.. The bound contribution in this case is $\alpha_s = 1.85650$ a.u. and the continuum is $\alpha_s = 3.41980$ a.u.. For a well depth of $V_0 = 0.302$ a.u. and screening length between $0.1 < \lambda < 1$ a.u., the static polarizability remains almost constant with a value of $\alpha_s = 1250$ a.u.. This increment in α_s is due to the weakening of the plasma interaction on the 1s and 2p states confined in the endohedral cavity, as confirmed in Figs. 2(b), 3(b) and 5(b), such that now the bound transition is the principal contribution to α_s. When $\lambda_D = 1$ a.u., we obtain that $\alpha_s = 1076.72239$, where $\alpha_s = 1074.06865$ a.u. is the contribution from the bound spectrum and $\alpha_s = 2.65374$ a.u. from the continuum states. For $\lambda_D \to \infty$ a.u. and $V_0 = 0.302$ a.u., the static polarizability is 5.03724 a.u.. In this case the plasma interaction competes with the endohedral well depth attraction, with an abrupt change of the static polarizability for

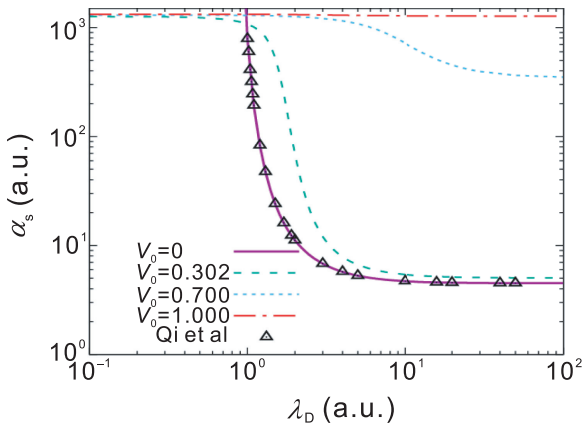

Fig. 8. Static dipole polarizability, α_s, for a H atom confined by an endohedral cavity in a Debye-Hückel plasma as a function of screening length, -λ_D, for several well depths V_0. The (△) symbols are the theoretical results from Qi et al. [16] for only plasma ($V_0 = 0$ a.u.). See text for details.

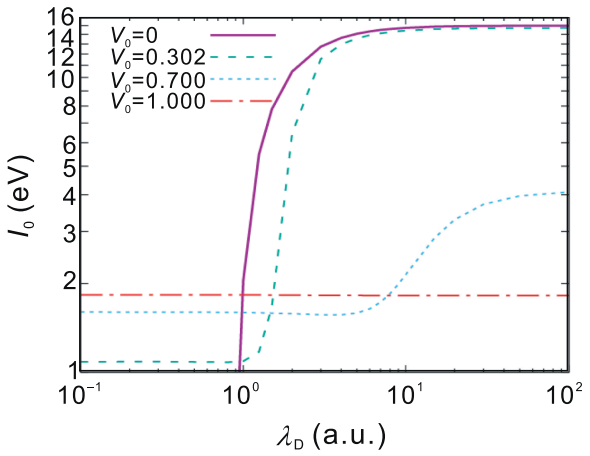

Fig. 9. Mean excitation energy, I_0, for an H atom confined by an endohedral cavity in a Debye-Hückel plasma as a function of screening length, λ_D, for several well depths V_0. The (△) symbols are the theoretical results from Qi et al. [16] for only plasma ($V_0 = 0$ a.u.). See text for details.

values around $0.8 < \lambda_D < 8$ a.u.. For a well depth of $V_0 = 0.7$ a.u., we observe a reduction of the abrupt change in the static polarizability, consequence of the fact that the energy levels are almost confined in the endohedral cage with a minimal effect from the Debye-Hückel interaction for all screening lengths. In Fig. 8, for $V_0 = 0.7$ a.u. and $0.1 < \lambda_D < 3$, we show that $\alpha_s = 1280$ a.u., and for $\lambda_D \to \infty$ a.u. a value of $\alpha_s = 345.91435$ a.u. is found. For $\lambda_D = 1.0$ a.u., $\alpha_s = 1290.29774$ a.u. where the bound contribution is $\alpha_s = 1289.34587$ a.u. and the continuum is $\alpha_s = 0.95187$ a.u.. When the well depth is increased to $V_0 = 1$ a.u., we observe a soft decrease from a value around $\alpha_s = 1321$ a.u. at $\lambda_D = 0.1$ a.u. to $\alpha_s = 1272$ a.u. at $\lambda_D \to \infty$ a.u., that is, a weak dependence on the plasma interaction. For $\lambda_D = 1.0$ a.u., we obtain $\alpha_s = 1320.17687$ a.u. where the bound contribution is $\alpha_s = 1319.66727$ a.u. and the continuum is $\alpha_s = 0.50960$ a.u.. Here, the 1s and 2p states are completely bound in the endohedral cavity, and no influence of the screening potential is observed. Consequently, the behavior of the α_s is due to the competition between the endohedral cavity and the Debye-Hückel interaction on the f_{2p} transition with a dominant contribution from the bound states as the cavity depth V_0 increases.

3.3.3. Mean excitation energy

In Fig. 9, we show the mean excitation energy, I_0, as a function of the screening length λ_D for several well depths V_0.

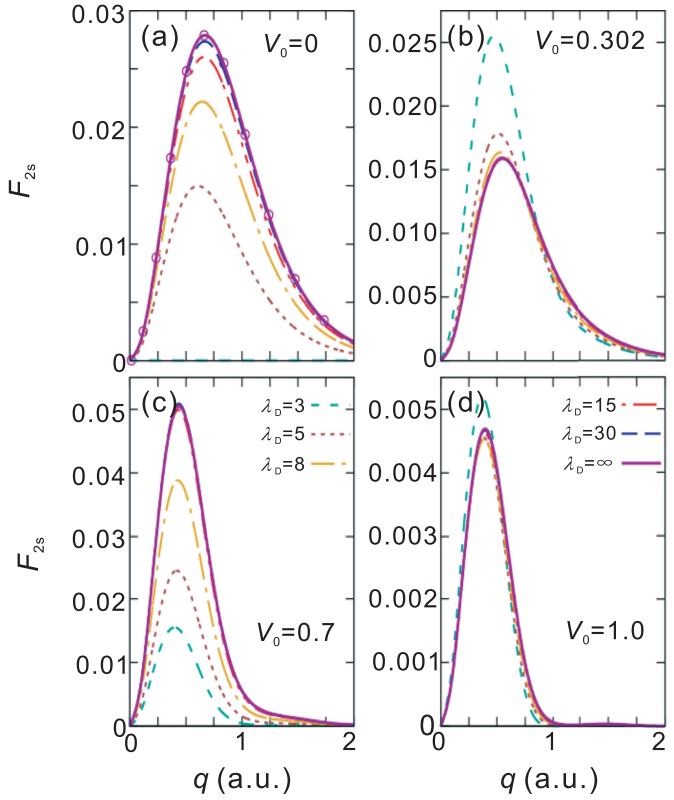

Fig. 10. Generalized oscillator strength for the 1s→2s transition, $F_{2s}(q)$, for atomic hydrogen confined by an endohedral cavity embedded in a Debye-Hückel plasma, as a function of the momentum transfer, q, for several well depths V_0 and screening lengths λ_D. We show the results for well depths: (a) $V_0 = 0.0$, (b) 0.302, (c) 0.7, and (d) 1.0 a.u. and selected screening lengths $\lambda_D = 3$, 5, 8, 15, 30, and ∞ a.u.. The (∘) symbols are the analytic results for the free hydrogen atom.

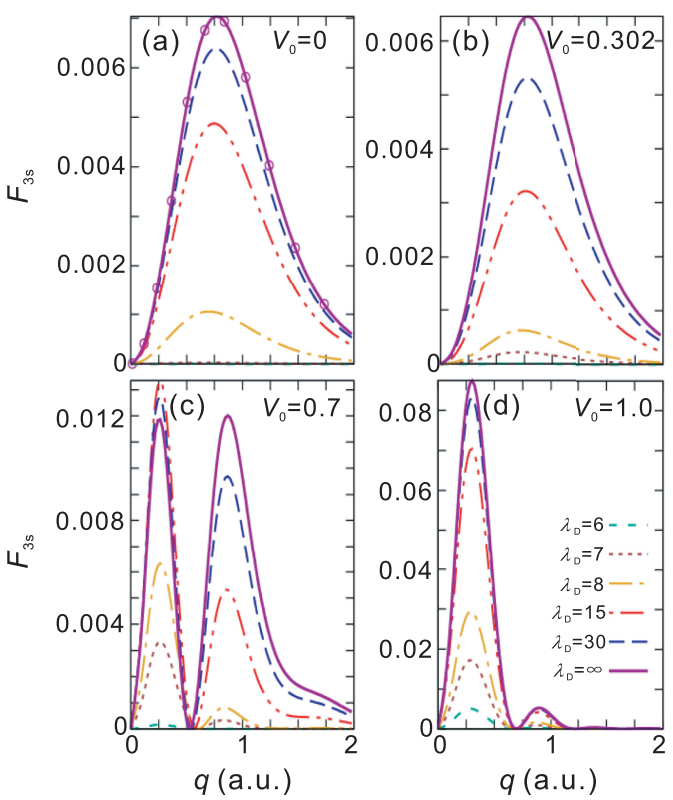

Fig. 11. Generalized oscillator strength for the 1s→3s transition, $F_{3s}(q)$, for atomic hydrogen confined by an endohedral cavity embedded in a Debye-Hückel plasma, as a function of the momentum transfer, q, for several well depths V_0 and screening lengths λ_D. We show the results for well depths: (a) $V_0 = 0.0$, (b) 0.302, (c) 0.7, and (d) 1.0 a.u. and selected screening lengths $\lambda_D = 3$, 5, 8, 15, 30, and ∞ a.u.. The (∘) symbols are the analytic results for the free hydrogen atom.

As we observe from the figure, the behavior of I_0 is similar to the static polarizability results reported in Fig. 8. In absence of the endohedral cavity ($V_0 = 0$ a.u.) and for $\lambda_D \to \infty$ a.u., we obtain the free hydrogen result of $I_0 = 14.993$ eV in agreement with the results of Cabrera-Trujillo and Cruz [57]. As the plasma interaction gets weak (diminishing of λ_D), the mean excitation energy decreases from $I_0 = 14.73608$ eV at $\lambda_D = 10$ a.u. to $I_0 = 14.07221$ eV at $\lambda_D = 5$ a.u.. When the cavity is present with $V_0 = 0.302$ a.u., we observe a constant value of $I_0 = 1.08$ eV for values of $\lambda_D < 1$ a.u.. Once again, the abrupt change is given at around $1 < \lambda_D < 10$ a.u. where the confinement effects of the endohedral cavity overtake the weak plasma interaction. When the well depth is $V_0 = 0.7$ a.u., the mean excitation energy is constant around $I_0 = 1.59$ eV for values of screening length $\lambda_D < 1.25$ a.u.. For this case, we have that the 1s and 2p states are partially and completely confined, respectively, in the endohedral cage. When the screening influence becomes weak (low λ_D values), the 1s and 2p energy levels are confined completely by the endohedral cage and we observe a constant value for I_0. In the case of $\lambda_D \to \infty$ a.u., we report a value of $I_0 = 4.12728$ eV. For $V_0 = 1$ a.u., the mean excitation energy is almost constant with a value of $I_0 = 1.830169$ a.u. at $\lambda_D = 0.1$ a.u. and $I_0 = 1.81943$ a.u. at $\lambda_D \to \infty$ a.u.. This behavior is attributed to the fact that the electron is strongly confined by the endohedral cavity with a minimal influence from the plasma interaction. This also implies that for low λ_D values, the stopping cross section will increase (see below) for high collision energies where Bethe's approximation is fulfilled.

3.4. GOS-dependent properties

3.4.1. Generalized oscillator strength

In Fig. 10, we show the GOS results for the 1s→2s, F_{2s}, transition as a function of the transferred momentum, q, for several well depths and selected screening lengths. In Fig. 10(a), we observe a decrease of the F_{2s} curve when the screening length is reduced, for $V_0 = 0$ a.u.. We observe that there is no F_{2s} contribution for screening lengths lower than $\lambda_D = 3.2601$ a.u., consequence of the delocalization of the 2s level, as we report in Fig. 2(a). For $\lambda_D > 15$ a.u., the curve is similar to the free case, i.e. there is a weak plasma influence on the hydrogen atom that modifies slightly the GOS. The (∘) symbols are the analytic GOS results for the free hydrogen atom [41,44] (i.e. $V_0 = 0$ and $\lambda_D \to \infty$ a.u.) showing an

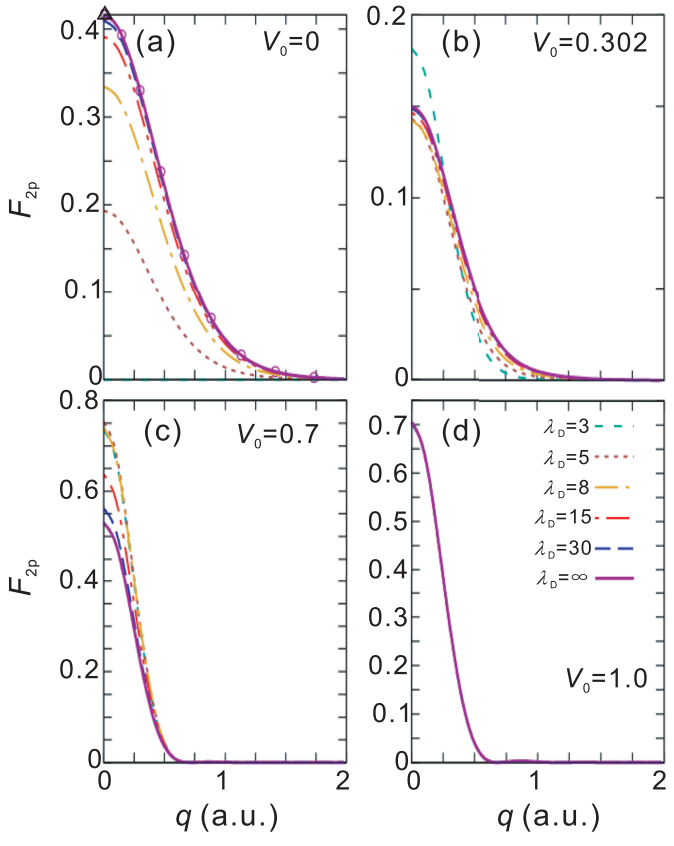

Fig. 12. Generalized oscillator strength for the 1s→2p transition, $F_{2p}(q)$, for atomic hydrogen confined by an endohedral cavity embedded in a Debye-Hückel plasma, as a function of the momentum transfer, q, for several well depths V_0 and screening lengths λ_D. We show the results for well depths: (a) $V_0 = 0.0$, (b) 0.302, (c) 0.7, and (d) 1.0 a.u. and selected screening lengths $\lambda_D = 3$, 5, 8, 15, 30, and ∞ a.u.. The (∘) symbols are the analytic results for the free hydrogen atom. The (△) symbol is the result for a free hydrogen atom at $q = 0$ a.u. ($f_{2p} = 0.41619$).

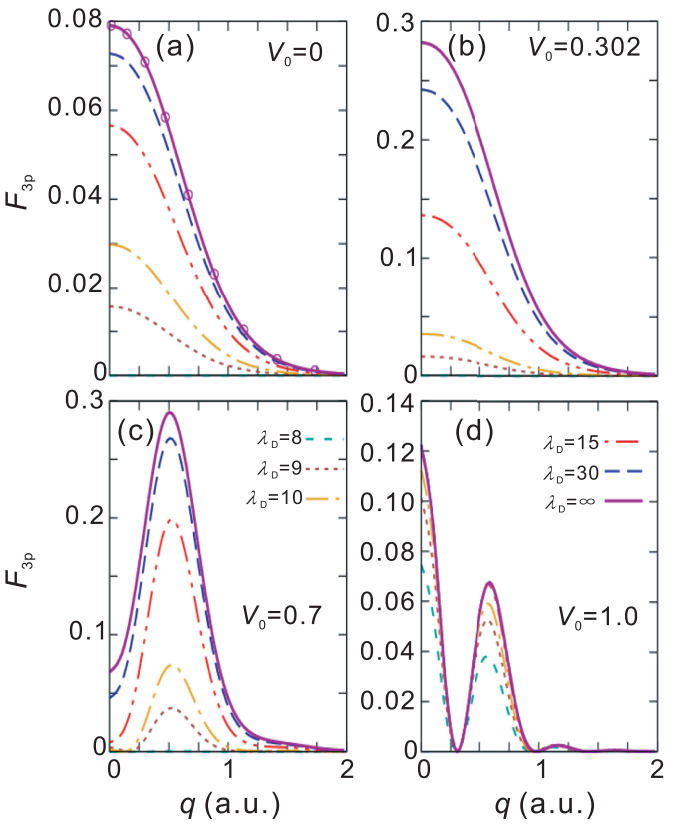

Fig. 13. Generalized oscillator strength for the 1s→3p transition, $F_{3p}(q)$, for atomic hydrogen confined by an endohedral cavity embedded in a Debye-Hückel plasma, as a function of the momentum transfer, q, for several well depths V_0 and screening lengths λ_D. We show the results for well depths: (a) $V_0 = 0.0$, (b) 0.302, (c) 0.7, and (d) 1.0 a.u. and selected screening lengths $\lambda_D = 3$, 5, 8, 15, 30, and ∞ a.u.. The (∘) symbols are the analytic results for the free hydrogen atom.

excellent agreement with our numerical calculation. In Fig. 10(b), when the cavity is present with $V_0 = 0.302$ a.u., the effect of the plasma interaction is to increase F_{2s} as the plasma screening length decreases, contrary to the case for $V_0 = 0$ a.u.. For a well depth of $V_0 = 0.7$ a.u., corresponding to the first avoided crossing of the pure endohedral hydrogen atom, the F_{2s} decreases smoothly with the decrease of the screening length but with a higher contribution than the case $V_0 = 0$. Fig. 10(d) shows the results for $V_0 = 1.0$ a.u., where the F_{2s} increases as the plasma screening length decreases. Recall here that the 1s and 2s energy levels are confined in the endohedral cavity.

In Fig. 11, we show the GOS for the $1s \rightarrow 3s$, F_{3s}, transition for selected potential well depths and screening lengths as a function of q. In Fig. 11(a), we show the F_{3s} results for a well depth of $V_0 = 0$ a.u., observing that there is no contribution to the GOS for $\lambda_D < 8$ a.u., as the 3s-excited state becomes delocalized (see Fig. 2(a)). For larger values of $\lambda_D > 8$ a.u., the F_{3s} curve increases softly until reaching the value of the free case. The ($\circ$) symbols are the analytic results for the free hydrogen atom [41] in excellent agreement with our numerical calculations. In Fig. 11(b), we show the effects of the plasma in the presence of the endohedral cavity for $V_0 = 0.302$ a.u.. Here, we observe an increase of the F_{3s} for $\lambda_D > 7$ a.u.. In Fig. 11(c), we observe the appearance of a minimum around $q = 0.5$ a.u., for $V_0 = 0.7$ a.u.. The F_{3s} intensity is reduced as the screening length is decreased. From Fig. 11(c), we observe a small contribution for $\lambda_D = 6$ a.u. of the 3s state which starts to be delocalized. When the well depth is increased to $V_0 = 1.0$ a.u., we observe, in Fig. 11(d), that the second maximum has decreased in intensity. Furthermore, this transition has a large intensity as the endohedral cavity deepens. As before, the F_{3s} curve decreases as the plasma screening length is decreased.

In Fig. 12, we show the GOS for the $1s \rightarrow 2p$, F_{2p}, transition for selected potential well depths and screening lengths as a function of transferred momentum q. In Fig. 12(a), for $V_0 = 0$ a.u., we observe a smooth decrease of the F_{2p} curve as the screening length is decreased. We notice that F_{2p} is negligible for $\lambda_D < 4.54257$ a.u. due to the delocalization of the 2p state. Once again, the ($\circ$) symbols are the analytic results for the free hydrogen atom [41] in excellent agreement with our

Table 3
Generalized oscillator strength for the $1s \rightarrow 2s$ and 3s transitions of a confined hydrogen atom by an endohedral cage embedded in a Debye-Hückel plasma as a function of the momentum transfer q for several well depths V_0 and screening lengths λ_D.

V_0 (a.u.)	λ_D (a.u.)	F_{2s}										
		q (a.u.)										
		0.0	0.2	0.4	0.6	0.8	1.0	1.2	1.4	1.6	1.8	2.0
	3	0.00000	0.00000	0.00000	0.00000	0.00000	0.00000	0.00000	0.00000	0.00000	0.00000	0.00000
0.0	8	0.00000	0.00575	0.01642	0.02201	0.02038	0.01518	0.00991	0.00598	0.00345	0.00195	0.00110
	15	0.00000	0.00637	0.01859	0.02562	0.02440	0.01863	0.01241	0.00760	0.00444	0.00253	0.00143
	30	0.00000	0.00658	0.01932	0.02686	0.02582	0.01988	0.01333	0.08212	0.00482	0.00275	0.00156
	3	0.00000	0.01072	0.02438	0.02254	0.01310	0.00625	0.00306	0.00165	0.00091	0.00005	0.00003
0.302	8	0.00000	0.00570	0.01446	0.01591	0.01150	0.00678	0.00379	0.00215	0.00122	0.00067	0.00037
	15	0.00000	0.00536	0.01383	0.01568	0.01175	0.00717	0.00411	0.00236	0.00134	0.00075	0.00041
	30	0.00000	0.00526	0.01368	0.01567	0.01189	0.00734	0.00424	0.00244	0.00140	0.00078	0.00043
	3	0.00000	0.00819	0.01554	0.00969	0.00270	0.00046	0.00016	0.00015	0.00011	0.00004	0.00001
0.7	8	0.00000	0.01844	0.03847	0.02908	0.01160	0.00340	0.00136	0.00090	0.00059	0.00028	0.00012
	15	0.00000	0.02321	0.04926	0.03851	0.01626	0.00514	0.00211	0.00136	0.00087	0.00043	0.00019
	30	0.00000	0.02347	0.05012	0.03965	0.01708	0.00554	0.00230	0.00146	0.00093	0.00047	0.00021
	3	0.00000	0.00304	0.00511	0.00233	0.00026	0.00000	0.00000	0.00000	0.00000	0.00000	0.00000
1.0	8	0.00000	0.00247	0.00452	0.00253	0.00051	0.00004	0.00000	0.00003	0.00002	0.00000	0.00000
	15	0.00000	0.00248	0.00461	0.00267	0.00058	0.00005	0.00001	0.00003	0.00003	0.00000	0.00000
	30	0.00000	0.00249	0.00466	0.00274	0.00062	0.00006	0.00002	0.00003	0.00003	0.00000	0.00000
		F_{3s}										
	3	0.00000	0.00001	0.00003	0.00003	0.00002	0.00002	0.00000	0.00000	0.00000	0.00000	0.00000
0.0	8	0.00000	0.00022	0.00068	0.00101	0.00102	0.00080	0.00054	0.00034	0.00020	0.00011	0.00006
	15	0.00000	0.00085	0.00282	0.00449	0.00483	0.00403	0.00285	0.00182	0.00110	0.00063	0.00036
	30	0.00000	0.00105	0.00355	0.00577	0.00636	0.00542	0.00390	0.00251	0.00152	0.00088	0.00051
	3	–	–	–	–	–	–	–	–	–	–	–
0.302	8	0.00000	0.00008	0.00033	0.00057	0.00061	0.00047	0.00031	0.00019	0.00011	0.00007	0.00004
	15	0.00000	0.00041	0.00160	0.00285	0.00321	0.00266	0.00185	0.00117	0.00070	0.00041	0.00023
	30	0.00000	0.00007	0.00257	0.00463	0.00530	0.00450	0.00318	0.00203	0.00123	0.00072	0.00041
	3	–	–	–	–	–	–	–	–	–	–	–
0.7	8	0.00000	0.00550	0.00358	0.00000	0.00078	0.00043	0.00006	0.00001	0.00003	0.00003	0.00001
	15	0.00000	0.01166	0.00700	0.00022	0.00496	0.00387	0.00130	0.00053	0.00045	0.00037	0.00020
	30	0.00000	0.01128	0.00593	0.00098	0.00899	0.00764	0.00317	0.00145	0.00107	0.00082	0.00045
	3	–	–	–	–	–	–	–	–	–	–	–
1.0	8	0.00000	0.02321	0.02179	0.00136	0.00132	0.00086	0.00000	0.00127	0.00000	0.00003	0.00000
	15	0.00000	0.05410	0.05465	0.00455	0.00284	0.00254	0.00000	0.00030	0.00001	0.00007	0.00003
	30	0.00000	0.06332	0.06554	0.00597	0.00321	0.00321	0.00000	0.00034	0.00002	0.00009	0.00004

numerical calculations. The ($\triangle$) symbol at $q = 0$ for F_{2p} and $V_0 = 0$ a.u. correspond to $f_{2p} = 0.41619$. When the well depth is increased to $V_0 = 0.302$ a.u., we observe a small effect of the plasma interaction in comparison with the free case. Furthermore, we observe a noticeable decrease of the F_{2p} intensity as compared to the free hydrogen case. This is due to the fact that the 2p state is almost confined by the endohedral potential, independently of the screening length. In Fig. 12(c), F_{2p} increases slightly as the screening length decreases. However, the intensity line has grown in comparison to the previous two cases. In Fig. 12(d), we observe that the plasma influence on the F_{2p} is negligible. The F_{2p} intensity remains the same for all values of the screening length. In this case, the electron is strongly bound in the cavity region and the plasma screening environment effects are negligible. However, the intensity line is stronger than in the previous cases.

In Fig. 13, we show the GOS for the $1s \rightarrow 3p$ transition, F_{3p}, for selected potential well depths and screening lengths as a function of the transferred momentum q. In Fig. 13(a), we show the case $V_0 = 0$ a.u., observing a decrease of the F_{3p} intensity as the plasma screening length is decreased. Notice that F_{3p} is negligible for screening lengths $\lambda_D = 8$ a.u.. The latter is attributed to the delocalization of the 3p energy level for values lower than $\lambda_D < 8.84610$ a.u. as reported in Table 1. As before, the ($\circ$) symbols are the analytic results for the free case. In Fig. 13(b), for a well depth of $V_0 = 0.302$ a.u., we observe a significant increase of the F_{3p} curve by a factor of 3 in comparison with Fig. 13(a). In Fig. 13(c), near the first avoided crossing of a H atom in an endohedral cavity, we observe a maximum at around $q = 0.5$ a.u.. With the decrease of the screening length, the F_{3p} curve decreases. In Fig. 13(d), we observe the appearance of an oscillatory behavior in the F_{3p} curve as a function of q. For screening lengths $\lambda_D > 10$ a.u., we observe that the influence of the Debye-Hückel plasma on the endohedral H atom is negligible.

Consequently, we state that the GOS distributions are modified by the presence of the plasma environment producing a decrease of the F_{ns} curves as the screening length decreased meanwhile the F_{np} increases. This effect will be relevant in the behavior of the electronic stopping cross-section and GOS-dependent properties.

Table 4
Generalized oscillator strength for the $1s \rightarrow 2p$ and 3p transitions of a confined hydrogen atom by an endohedral cage embedded in a Debye-Hückel plasma as a function of the momentum transfer q for several well depths V_0 and screening lengths λ_D.

V_0 (a.u.)	λ_D (a.u.)	F_{2p}										
		q (a.u.)										
		0.0	0.2	0.4	0.6	0.8	1.0	1.2	1.4	1.6	1.8	2.0
	3	–	–	–	–	–	–	–	–	–	–	–
0.0	8	0.33444	0.29736	0.21209	0.12605	0.06549	0.03116	0.01410	0.00624	0.00276	0.00123	0.00056
	15	0.39147	0.35097	0.25594	0.15665	0.08389	0.04099	0.01895	0.00853	0.00382	0.00172	0.00079
	30	0.40953	0.36811	0.27028	0.16697	0.09028	0.04450	0.02072	0.00938	0.00421	0.00190	0.00087
	3	0.18145	0.13635	0.05806	0.01451	0.00263	0.00067	0.00034	0.00018	0.00006	0.00002	0.00000
0.302	8	0.14226	0.11610	0.06434	0.02603	0.00902	0.00335	0.00146	0.00066	0.00028	0.00011	0.00005
	15	0.14646	0.12118	0.06999	0.03028	0.01133	0.00441	0.00194	0.00088	0.00038	0.00015	0.00007
	30	0.14893	0.12381	0.07254	0.03209	0.01231	0.00487	0.00215	0.00097	0.00042	0.00017	0.00008
	3	0.73564	0.49646	0.13316	0.00517	0.00216	0.00112	0.00002	0.00018	0.00000	0.00002	0.00000
0.7	8	0.73967	0.50336	0.13975	0.00656	0.00170	0.00103	0.00002	0.00019	0.00000	0.00002	0.00000
	15	0.63689	0.43581	0.12390	0.00663	0.00114	0.00077	0.00003	0.00017	0.00001	0.00001	0.00000
	30	0.56138	0.38534	0.11103	0.00638	0.00084	0.00061	0.00003	0.00016	0.00001	0.00000	0.00000
	3	0.70140	0.47573	0.12855	0.00459	0.00268	0.00132	0.00004	0.00026	0.00000	0.00004	0.00000
1.0	8	0.70370	0.47833	0.13035	0.00486	0.00263	0.00135	0.00003	0.00026	0.00000	0.00004	0.00000
	15	0.70443	0.47912	0.13089	0.00494	0.00261	0.00136	0.00003	0.00026	0.00000	0.00004	0.00001
	30	0.70473	0.47945	0.13111	0.00497	0.00260	0.00137	0.00003	0.00026	0.00000	0.00004	0.00001
		F_{3p}										
	3	–	–	–	–	–	–	–	–	–	–	–
0.0	8	–	–	–	–	–	–	–	–	–	–	–
	15	0.05658	0.05342	0.04414	0.03112	0.01880	0.01004	0.00493	0.00231	0.00106	0.00048	0.00022
	30	0.07275	0.06920	0.05830	0.04216	0.02612	0.01425	0.00711	0.00337	0.00156	0.00072	0.00033
	3	–	–	–	–	–	–	–	–	–	–	–
0.302	8	–	–	–	–	–	–	–	–	–	–	–
	15	0.13657	0.13054	0.11030	0.07850	0.04693	0.02457	0.01192	0.00559	0.00258	0.00118	0.00054
	30	0.24251	0.23210	0.19772	0.14330	0.08765	0.04682	0.02299	0.01086	0.00505	0.00233	0.00107
	3	–	–	–	–	–	–	–	–	–	–	–
0.7	8	0.00003	0.00000	0.00009	0.00010	0.00003	0.00000	0.00000	0.00000	0.00000	0.00000	0.00000
	15	0.00796	0.04410	0.16308	0.18536	0.08608	0.02160	0.00604	0.00396	0.00295	0.00133	0.00039
	30	0.00459	0.10152	0.23555	0.24908	0.12657	0.03889	0.01255	0.00717	0.00475	0.00222	0.00075
	3	–	–	–	–	–	–	–	–	–	–	–
1.0	8	0.07464	0.01665	0.01391	0.03695	0.00748	0.00049	0.00137	0.00000	0.00030	0.00005	0.00003
	15	0.12271	0.02991	0.02036	0.06597	0.01786	0.00023	0.00237	0.00004	0.00049	0.00014	0.00003
	30	0.12223	0.03036	0.01980	0.06727	0.01951	0.00012	0.00235	0.00005	0.00048	0.00016	0.00002

For reference purposes, in Tables 3 and 4, we report the GOS for the 1s→2s, 2p, 3s, and 3p transitions for selected sets of well depths V_0, screening length λ_D, and transferred momentum q.

3.4.2. Electronic stopping cross section

In Fig. 14, we show the electronic stopping cross section (SCS) for protons colliding with atomic hydrogen encaged by an endohedral cavity and embedded in a Debye-Hückel plasma. In this case the assumption in our model is that the projectile momentum transfer goes only to the active electron in the hydrogen target and not into the endohedral cavity. In Fig. 14(a), we show the results for $V_0 = 0$ a.u. where the hydrogen atom is subjected only to the Debye-Hückel plasma interaction. The largest effect of the plasma environment is in the low-to-intermediate energy collision region and for small screening length values. As the plasma interaction is decreased, the energy deposited by the ions into the hydrogen system increases slightly. We find that only for $\lambda_D < 8$ a.u., the plasma interaction affects the high energy region of the SCS. This is because for low values of the screening length the bound states are near the delocalization threshold meaning a higher absorption of the projectile energy. We compare our results to those of a free hydrogen as reported by Bichsel [58] based in the same first Born approximation ((∘) symbols) observing an excellent agreement to our free case results, $V_0 =$ 0 a.u. and $\lambda_D \to \infty$ (solid line). In Fig. 14(b), we show the results for $V_0 = 0.302$ a.u., observing a significant change in the SCS for low-to-intermediate collision energy for $\lambda_D < 3$ a.u.. In Fig. 14(c), we show the results for $V_0 = 0.7$ a.u., i.e. a well depth near the first avoided crossing for an H atom confined by an endohedral cavity without plasma interaction, observing an increase of the SCS for $\lambda_D \to \infty$ (solid line) in comparison with the previous results of Fig. 14(a) and (b) for intermediate-to-high projectile energies. For comparison purposes, we show the free case result (solid thin line) in Fig. 14(c) and (d). Also, we observe a slight effect of the plasma interaction on the H atom stopping cross section for all projectile energies. In Fig. 14(d), we show the results for $V_0 =$ 1.0 a.u., where one observes that the effect of the plasma influence on the electronic SCS is negligible. As the endohedral cavity potential well increases, more bound states appear below the delocalization threshold with the dominant transition becoming the 1s→2p, thus increasing the SCS. Thus, the stronger effect of the plasma is for shallow cavities. For deep cavities, the effect of the plasma is negligible with a predominant contribution only from the endohedral cavity.

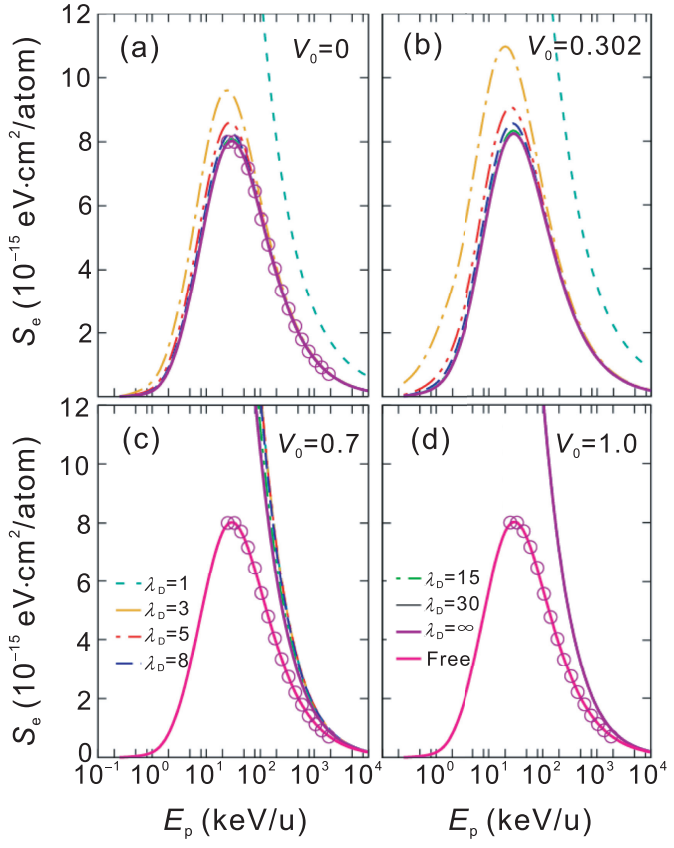

Fig. 14. Electronic stopping cross section for protons colliding with atomic hydrogen encaged by an endohedral cavity and embedded in Debye-Hückel plasma as a function of the projectile initial kinetic energy for several selected confinement well depths V_0 and plasma screening lengths λ_D. In (a) $V_0 = 0.0$, (b) $V_0 = 0.302$, (c) $V_0 = 0.7$, and (d) $V_0 = 1.0$ a.u.. The (∘) symbols are the free atomic hydrogen theoretical results of Bichsel [58].

4. Conclusions

In this work, we report the effects of the spatial confinement produced by an endohedral cavity on a hydrogen atom embedded in a plasma on properties dependent on the dipole and generalized oscillator strength, i.e. hydrogen atom in extreme conditions. We have used the Woods-Saxon model potential to describe the static endohedral cage. The plasma interaction is described by the Debye-Hückel screening potential. It is found that the energy levels and wave-functions are modified drastically. With the increase of the endohedral well depth and the decrease of the plasma screening length, the electron in the hydrogen atom is bound into the cavity region. We also find a delocalization of the 1s and 2p energy levels for screening lengths lower than $\lambda_D < 1$ a.u., for low values of V_0. Consequently, the DOS and GOS are modified strongly as these parameters are varied, showing that Copper structures in the photo-ionization cross section move towards high photo-ionization energies as λ_D decreases, as well as a drastic change on the static dipole polarizability and mean excitation energy. We find that the effect of the plasma is to weaken the 1s→2p transition as λ_D decreases, while adding the endohedral cavity strengthen the transition emission as λ_D decreases, becoming the dominant emission line. In the case of the photo-ionization, we find that the Cooper resonances are displaced towards high photo-electron energy as λ_D is decreased. We also find that the hydrogen GOS confined in a plasma environment produces a decrease of the F_{ns} as the screening length decreases meanwhile the F_{np} increases. Thus, we find a strong competition between the effects of the plasma interaction and those of the static endohedral cavity which modify accordingly the electronic properties of the system.

We hope our findings motivate further study on this novel system in extreme conditions either with theoretical or experimental work.

Conflict of interest

The authors have no conflict of interest on this original research.

Acknowledgments

This work was supported by grants DGAPA-UNAM PAPIIT-IN-106-617 and LANCAD-UNAM-DGTIC-228 granted to RCT. CMF would like to thank CONACyT scholarship with CVU 424130. We acknowledge the computer center at ICF-UNAM and to Reyes Garcia for computational assistance.

References

[1] D. Salzmann (Ed.), Atomic Physics in Hot Plasmas, Oxford University Press, Oxford, 1998.
[2] R. Janev, S. Zhang, J. Wang, Review of quantum collision dynamics in debye plasmas, Matter Radiat. Extrem. 1 (5) (2016) 237−248, https://doi.org/10.1016/j.mre.2016.10.002.
[3] P.S. Committee (Ed.), Plasma Science: From Fundamental Research to Technological Applications, first ed., National Academies Press, Washington, DC, 1995.
[4] K. Nishikawa, M. Wakatani (Eds.), Plasma Physics: Basic Theory with Fusion Applications, third ed., Springer-Verlag Berlin Heidelberg, Switzerland, 2000 https://doi.org/10.1007/978-3-662-04078-2. http://www.springer.com/us/book/9783540652854.
[5] O.V. Penkov, M. Khadem, W.-S. Lim, D.-E. Kim, A review of recent applications of atmospheric pressure plasma jets for materials processing, J. Coating Technol. Res. 12 (2) (2015) 225−235, https://doi.org/10.1007/s11998-014-9638-z.
[6] Y. Kuramitsu, Y. Sakawa, T. Morita, T. Ide, K. Nishio, et al., Laboratory investigations on the origins of cosmic rays, Plasma Phys. Contr. Fusion 54 (12) (2012) 124049, https://doi.org/10.1088/0741-3335/54/12/124049. http://stacks.iop.org/0741-3335/54/i=12/a=124049.
[7] M.S. Murillo, J.C. Weisheit, Dense plasmas, screened interactions, and atomic ionization, Phys. Rep. 302 (1) (1998) 1−65, https://doi.org/10.1016/S0370-1573(98)00017-9.
[8] A. Sil, S. Canuto, P. Mukherjee, Spectroscopy of confined atomic systems: effect of plasma, Adv. Quant. Chem. 58 (2009) 115−175, https://doi.org/10.1016/S0065-3276(09)00708-4. http://www.sciencedirect.com/science/article/pii/S0065327609007084.
[9] E. Hückel, P. Debye, The theory of electrolytes: I. Lowering of freezing point and related phenomena, Phys. Z 24 (1923) 185−206.
[10] Y.Y. Qi, J.G. Wang, R.K. Janev, Photoionization of hydrogen-like ions in dense quantum plasmas, Phys. Plasmas 24 (6) (2017) 062110, https://doi.org/10.1063/1.4985658.
[11] L.G. Stanton, M.S. Murillo, Unified description of linear screening in dense plasmas, Phys. Rev. E 91 (2015) 033104, https://doi.org/10.1103/PhysRevE.91.033104.
[12] G.P. Zhao, L. Liu, J.G. Wang, R.K. Janev, Spectral properties of hydrogen-like ions in finite-temperature quantum plasmas, Phys. Plasmas 24 (5) (2017) 053509, https://doi.org/10.1063/1.4982658.
[13] Y.Y. Qi, J.G. Wang, R.K. Janev, Dynamics of photoionization of hydrogenlike ions in debye plasmas, Phys. Rev. A 80 (2009) 063404, https://doi.org/10.1103/PhysRevA.80.063404.
[14] C.Y. Lin, Y.K. Ho, Effects of screened Coulomb (Yukawa) and exponential-cosine-screened Coulomb potentials on photoionization of H and He^+, Eur. Phys. J. D 57 (1) (2010) 21−26, https://doi.org/10.1140/epjd/e2010-00009-8.
[15] T.N. Chang, T.K. Fang, Atomic photoionization in a changing plasma environment, Phys. Rev. A 88 (2013) 023406, https://doi.org/10.1103/PhysRevA.88.023406.
[16] Y.Y. Qi, J.G. Wang, R.K. Janev, Static dipole polarizability of hydrogenlike ions in Debye plasmas, Phys. Rev. A 80 (2009) 032502, https://doi.org/10.1103/PhysRevA.80.032502.
[17] M. Das, Transition energies and polarizabilities of hydrogen like ions in plasma, Phys. Plasmas 19 (9) (2012) 092707, https://doi.org/10.1063/1.4754716.
[18] H.W. Li, S. Kar, Polarizabilities of Li and Na in debye plasmas, Phys. Plasmas 19 (7) (2012) 073303, https://doi.org/10.1063/1.4739229.
[19] H.-W. Li, S. Kar, P. Jiang, Calculations of dynamic dipole polarizabilities of Li and Na atoms in Debye plasma using the model potential technique, Int. J. Quant. Chem. 113 (10) (2013) 1493−1497, https://doi.org/10.1002/qua.24347.
[20] D.H.H. Hoffmann, K. Weyrich, H. Wahl, D. Gardés, R. Bimbot, C. Fleurier, Energy loss of heavy ions in a plasma target, Phys. Rev. A 42 (1990) 2313−2321, https://doi.org/10.1103/PhysRevA.42.2313.
[21] A.B. Zylstra, J.A. Frenje, P.E. Grabowski, C.K. Li, G.W. Collins, et al., Measurement of charged-particle stopping in warm dense plasma, Phys. Rev. Lett. 114 (2015) 215002, https://doi.org/10.1103/PhysRevLett.114.215002.
[22] G. Xu, M.D. Barriga-Carrasco, A. Blazevic, B. Borovkov, D. Casas, et al., Determination of hydrogen density by swift heavy ions, Phys. Rev. Lett. 119 (2017) 204801, https://doi.org/10.1103/PhysRevLett.119.204801.
[23] K.D. Sen (Ed.), Electronic Structure of Quantum Confined Atoms and Molecules, Springer International Publishing, Switzerland, 2014, https://doi.org/10.1007/978-3-319-09982-8.
[24] R.B. Ross, C.M. Cardona, D.M. Guldi, S.G. Sankaranarayanan, M.O. Reese, et al., Endohedral fullerenes for organic photovoltaic devices, Nat. Mater. 8 (3) (2014) 208−212, https://doi.org/10.1038/nmat2379.
[25] S. Ornes, Core concept: quantum dots, Proc. Natl. Acad. Sci. Unit. States Am. 113 (11) (2016) 2796−2797, https://doi.org/10.1073/pnas.1601852113. http://www.pnas.org/content/113/11/2796.short.
[26] O.V. Pupysheva, A.A. Farajian, B.I. Yakobson, Fullerene nanocage capacity for hydrogen storage, Nano Lett. 8 (3) (2008) 767−774, https://doi.org/10.1021/nl071436g pMID: 17924697. arXiv.
[27] J.A. Teprovich, A.L. Washington, J. Dixon, P.A. Ward, J.H. Christian, et al., Investigation of hydrogen induced fluorescence in C_60 and its potential use in luminescence down shifting applications, Nanoscale 8 (2016) 18760−18770, https://doi.org/10.1039/C6NR05998H.
[28] W. Jaskólski, Confined many-electron systems, Phys. Rep. 271 (1) (1996) 1−66, https://doi.org/10.1016/0370-1573(95)00070-4. http://www.sciencedirect.com/science/article/pii/0370157395000704.
[29] J.P. Connerade, V.K. Dolmatov, P.A. Lakshmi, The filling of shells in compressed atoms, J. Phys. B Atomic Mol. Opt. Phys. 33 (2) (2000) 251, https://doi.org/10.1088/0953-4075/33/2/310. http://stacks.iop.org/0953-4075/33/i=2/a=310.
[30] S.A. Cruz, J. Sabin, E. Brandas (Eds.), Advances in quantum chemistry, vol. 57, Elsevier, Amsterdam, 2009. http://www.sciencedirect.com/science/bookseries/00653276/57.
[31] S.A. Cruz, J. Sabin, E. Brandas (Eds.), Advances in Quantum Chemistry, vol. 58, Elsevier, Amsterdam, 2009. http://www.sciencedirect.com/science/bookseries/00653276/58.
[32] R.D. Woods, D.S. Saxon, Diffuse surface optical model for nucleon-nuclei scattering, Phys. Rev. 95 (1954) 577−578, https://doi.org/10.1103/PhysRev.95.577.
[33] V.K. Dolmatov, J.L. King, J.C. Oglesby, Diffuse versus square-well confining potentials in modelling $A@C_60$ atoms, J. Phys. B Atom. Mol. Opt. Phys. 45 (10) (2012) 105102. http://stacks.iop.org/0953-4075/45/i=10/a=105102.
[34] M.Y. Amusia, A.S. Baltenkov, L.V. Chernysheva, Z. Felfli, A.Z. Msezane, Dramatic distortion of the 4d giant resonance by the C_60

fullerene shell, J. Phys. B Atom. Mol. Opt. Phys. 38 (10) (2005) L169. http://stacks.iop.org/0953-4075/38/i=10/a=L06.

[35] V. Dolmatov, Photoionization of atoms encaged in spherical fullerenes, in: Advances in Quantum Chemistry, vol. 58, Academic Press, 2009, pp. 13−68, https://doi.org/10.1016/S0065-3276(09)00706-0. http://www.sciencedirect.com/science/article/pii/S0065327609007060.

[36] C.Y. Lin, Y.K. Ho, Photoionization of atoms encapsulated by cages using the power-exponential potential, J. Phys. B Atom. Mol. Opt. Phys. 45 (14) (2012) 145001. http://stacks.iop.org/0953-4075/45/i=14/a=145001.

[37] C.Y. Lin, Y.K. Ho, Photoionization of endohedral atoms in fullerene cages, Few Body Syst. 54 (1) (2013) 425−429, https://doi.org/10.1007/s00601-012-0405-3.

[38] C.Y. Lin, Y.K. Ho, Photoionization cross sections of hydrogen impurities in spherical quantum dots using the finite-element discrete-variable representation, Phys. Rev. A 84 (2011) 023407, https://doi.org/10.1103/PhysRevA.84.023407.

[39] E.K. Campbell, M. Holz, D. Gerlich, J.P. Maier, Laboratory confirmation of $C_6 0^+$ as the Carrier of two diffuse interstellar bands, Nature 523 (2015) 322, https://doi.org/10.1038/nature14566.

[40] C. Teske, Y. Liu, S. Blaes, J. Jacoby, Electron density and plasma dynamics of a spherical theta pinch, Phys. Plasmas 19 (3) (2012) 033505, https://doi.org/10.1063/1.3690107 arXiv.

[41] R. Cabrera-Trujillo, S.A. Cruz, Confinement approach to pressure effects on the dipole and the generalized oscillator strength of atomic hydrogen, Phys. Rev. A 87 (2013) 012502, https://doi.org/10.1103/PhysRevA.87.012502.

[42] S. Koonin, D.C. Meredith, Computational Physics: Fortran Version, Westview Press, 1998.

[43] H.A. Bethe, R. Jackiw (Eds.), Intermediate Quantum Mechanics, third ed., Westview Press, Boulder, Colorado, 1997. EE.UU.

[44] M. Inokuti, Inelastic collisions of fast charged particles with atoms and molecules-the bethe theory revisited, Rev. Mod. Phys. 43 (1971) 297−347, https://doi.org/10.1103/RevModPhys.43.297.

[45] H. Friedrich (Ed.), Theoretical Atomic Physics, third ed., Springer-Verlag Berlin Heidelberg, 2006 https://doi.org/10.1007/3-540-29278-0.

[46] L.M. Ugray, R.C. Shiell, Elucidating Fermi's golden rule via bound-to-bound transitions in a confined hydrogen atom, Am. J. Phys. 81 (3) (2013) 206−210, https://doi.org/10.1119/1.4773564.

[47] H. Bethe, Zur theorie des durchgangs schneller korpuskularstrahlen durch materie, Annalen der Physik 397 (3) (1930) 325−400, https://doi.org/10.1002/andp.19303970303.

[48] Y.B. Xu, M.Q. Tan, U. Becker, Oscillations in the photoionization cross section of C_{60}, Phys. Rev. Lett. 76 (1996) 3538−3541, https://doi.org/10.1103/PhysRevLett.76.3538.

[49] M.F. Hasoğlu, H.-L. Zhou, S.T. Manson, Correlation study of endohedrally confined alkaline-earth-metal atoms ($A@C_{60}$), Phys. Rev. A 93 (2016) 022512, https://doi.org/10.1103/PhysRevA.93.022512.

[50] S. Kang, Y.-C. Yang, J. He, F.-Q. Xiong, N. Xu, The hydrogen atom confined in both debye screening potential and impenetrable spherical box, Cent. Eur. J. Phys. 11 (5) (2013) 584−593, https://doi.org/10.2478/s11534-013-0230-4.

[51] S. Lumb, S. Lumb, V. Prasad, Photoexcitation and ionization of a hydrogen atom confined by a combined effect of a spherical box and debye plasma, Phys. Lett. A 379 (18) (2015) 1263−1269. https://doi.org/10.1016/j.physleta.2015.02.041. http://www.sciencedirect.com/science/article/pii/S0375960115002145.

[52] S. Lumb, S. Lumb, V. Nautiyal, Photoexcitation and ionization of hydrogen atom confined in debye environment, Eur. Phys. J. D 69 (7) (2015) 176, https://doi.org/10.1140/epjd/e2015-60136-2.

[53] B. Saha, P.K. Mukherjee, G.H.F. Diercksen, Energy levels and structural properties of compressed hydrogen atom under Debye screening, Astron. Astrophys. 396 (2002) 337, https://doi.org/10.1051/0004-6361:20021350.

[54] J.W. Cooper, Photoionization from outer atomic subshells. A model study, Phys. Rev. 128 (1962) 681−693, https://doi.org/10.1103/PhysRev.128.681.

[55] J.W. Cooper, Interaction of maxima in the absorption of soft X rays, Phys. Rev. Lett. 13 (1964) 762−764, https://doi.org/10.1103/PhysRevLett.13.762.

[56] M.Y. Amusia, Photoionization and vacancy decay of endohedral atoms, J. Electron. Spectrosc. Relat. Phenom. 161 (1) (2007) 112−120, https://doi.org/10.1016/j.elspec.2007.04.004.

[57] R. Cabrera-Trujillo, S. Cruz, Accurate evaluation of pressure effects on the electronic stopping cross section and mean excitation energy of atomic hydrogen beyond the bethe approximation, Nucl. Instrum. Methods Phys. Res. Sect. B Beam Interact. Mater. Atoms 320 (2014) 51−56, https://doi.org/10.1016/j.nimb.2013.12.011. http://www.sciencedirect.com/science/article/pii/S0168583X13011725.

[58] H. Bichsel, Stopping power of hydrogen atoms, Phys. Rev. A 43 (1991) 4030−4031, https://doi.org/10.1103/PhysRevA.43.4030.